

Bubble nucleation in spherical liquid cavity wrapped by elastic medium

Xian-Mei Zhang(张先梅), Fan Li(李凡), Cheng-Hui Wang(王成会), Jing Hu(胡静), Run-Yang Mo(莫润阳), Zhuang-Zhi Shen(沈壮志), Jian-Zhong Guo(郭建中), and Shu-Yu Lin(林书玉)

Citation: Chin. Phys. B, 2023, 32 (**6**): 064303. DOI: 10.1088/1674-1056/acaa30
Journal homepage: http://cpb.iphy.ac.cn; http://iopscience.iop.org/cpb

What follows is a list of articles you may be interested in

Effects of adjacent bubble on spatiotemporal evolutions of mechanical stresses surrounding bubbles oscillating in tissues

Qing-Qin Zou(邹青钦), Shuang Lei(雷双), Zhang-Yong Li(李章勇), and Dui Qin(秦对)
Chin. Phys. B, 2023, 32 (**1**): 014302. DOI: 10.1088/1674-1056/ac70ba

Effect of porous surface layer on wave propagation in elastic cylinder immersed in fluid

Na-Na Su(苏娜娜), Qing-Bang Han(韩庆邦), Ming-Lei Shan(单鸣雷), and Cheng Yin(殷澄)
Chin. Phys. B, 2023, 32 (**1**): 014301. DOI: 10.1088/1674-1056/ac6ee6

Controlling acoustic orbital angular momentum with artificial structures: From physics to application

Wei Wang(王未), Jingjing Liu(刘京京), Bin Liang (梁彬), and Jianchun Cheng(程建春)
Chin. Phys. B, 2022, 31 (**9**): 094302. DOI: 10.1088/1674-1056/ac7868

Sound-transparent anisotropic media for backscattering-immune wave manipulation

Wei-Wei Kan(阚威威), Qiu-Yu Li(李秋雨), and Lei Pan(潘蕾)
Chin. Phys. B, 2022, 31 (**8**): 084302. DOI: 10.1088/1674-1056/ac4904

Analysis on vibration characteristics of large-size rectangular piezoelectric composite plate based on quasi-periodic phononic crystal structure

Li-Qing Hu(胡理情), Sha Wang(王莎), and Shu-Yu Lin(林书玉)
Chin. Phys. B, 2022, 31 (**5**): 054302. DOI: 10.1088/1674-1056/ac3649

Bubble nucleation in spherical liquid cavity wrapped by elastic medium

Xian-Mei Zhang(张先梅), Fan Li(李凡), Cheng-Hui Wang(王成会)†, Jing Hu(胡静), Run-Yang Mo(莫润阳), Zhuang-Zhi Shen(沈壮志), Jian-Zhong Guo(郭建中), and Shu-Yu Lin(林书玉)

Institute of Shaanxi Key Laboratory of Ultrasonics, Shaanxi Normal University, Xi'an 710119, *China*

(Received 23 October 2022; revised manuscript received 7 December 2022; accepted manuscript online 9 December 2022)

According to classical nucleation theory, gas nuclei can generate and grow into a cavitation bubble when the liquid pressure exceeds a threshold. However, classical nucleation theory does not include boundary effects. An enclosed spherical liquid cavity surrounded by elastic medium is introduced to model the nucleation process in tissue. Based on the equilibrium pressure relationship of a quasi-static process, the expressions of the threshold and the modified nucleation rate are derived by considering the tissue elasticity. It is shown that the constraint plays an important role in the nucleation process. There is a positive correlation between nucleation threshold pressure and constraint, which can be enhanced by an increasing tissue elasticity and reducing the size of the cavity. Meanwhile, temperature is found to be a key parameter of nucleation process, and cavitation is more likely to occur in confined liquids at temperature $T > 100$ °C. In contrast, less influences are induced by these factors, such as bulk modulus, liquid cavity size, and acoustic frequency. Although these theoretical predictions of the thresholds have been demonstrated by many previous researches, much lower thresholds can be obtained in liquids containing dissolved gases, *e.g.*, the nucleation threshold is about −21 MPa in a liquid of 0.8-nm gas nuclei at room temperature. Moreover, when there is a gas nucleus of 20 nm, the theoretical threshold pressure might be less than 1 MPa.

Keywords: elastic confinement, liquid cavities, cavitation nucleation

PACS: 43.35.+d, 43.25.+y, 47.55.dp **DOI:** 10.1088/1674-1056/acaa30

1. Introduction

When the liquid pressure decreases to negative pressure, the gas nuclei will generate and grow into bubbles, and cavitation might be excited. Cavitation has been investigated for many years, and various models have been developed to describe the motion of bubbles in aqueous media,[1–3] near a rigid surface[4] and in a liquid cavity.[5,6] In recent years, ultrasonic cavitation has emerged in various medical applications as a way to influence matter noninvasively. The cavitation effects have been widely investigated and employed in different medical treatments, such as ablation of tumors,[7] fractionation of calculi[8] or tissue,[9] enhancement of permeability of cells for drug delivery,[10] non-invasive surgery,[11] contrast in ultrasound enhanced imaging,[12] and reversible opening of blood–brain barrier.[13] However, the key problem in the clinical application of ultrasound-induced cavitation is the high uncertainty of bubble nucleation,[14] which may be responsible for the slow development of cavitation-based ultrasound therapy compared to the use of thermal effects only. Indeed, the controlling bubble nucleation in living tissue is a significant challenge.[14]

The classical nucleation theory (CNT) provides an estimation of the tensile strength of a liquid, with a tensile threshold of about 140 MPa for water,[15] and alternative models predict much lower thresholds, in a range between 27 MPa and 100 MPa.[16] Nonetheless, the homogeneous cavitation threshold of pure water, measured at room temperature, ranges from 21 MPa to 30 MPa.[17–19] It has recently been shown that ultrasound cavitation can be modeled with the aid of CNT as long as the surface tension of water is corrected to an effective value.[19–21] However, boundary effects are not taken into account in the CNT and the physical feature of biological tissues is very complex. Therefore, it is not applicable to the localized cavitation nucleation of biological tissues. Nevertheless, the CNT is a widely preferred theory for the cavitation nucleation in soft tissues.[22,23] A phenomenological implementation of CNT is employed to investigate the energy requirements of bubble nucleation influenced by the high intensity focused ultrasound pressure field and temperature field.[24] This model can predict the spatial–temporal trends of nucleation in the focused acoustic fields, but it cannot answer the question about the physical mechanism of bubble growth. By combining the effects of the liquid viscosity and inertia with the classical nucleation theory through the Rayleigh–Plesset equation, a hydrodynamic model of ultrasound-induced nucleation was obtained, which makes it possible to ascertain the dominant mechanism of bubble nucleation.[25]

An intrinsic threshold of approximately 26 MPa–30 MPa was observed for water-based soft tissues and tissue phantoms by using a 1.1-MHz histotripsy transducer, whereas the threshold for tissue composed primarily of lipids was significantly low (about 15.4 MPa for adipose tissue),[20] which im-

†Corresponding author. E-mail: wangld001@snnu.edu.cn

© 2023 Chinese Physical Society and IOP Publishing Ltd

plies that tissue characteristics have a remarkable influence on the threshold pressure. It is found that tissue characteristics strongly affect histopathological treatment of porcine liver in vivo, with large hepatic vessels of high mechanical strength being preserved, while peripheral liver parenchyma of low mechanical strength was completely fractionated.[26] However, Maxwell *et al.*[20] measured the cavitation probability in tissue phantoms and soft tissues with a limited range of Young's moduli (≤ 36 kPa) at an ultrasound frequency (1.1 MHz), and they found that elasticity does not significantly change this threshold for cavitation but does change the dynamics of bubble growth and collapse. Vlaisavljevich *et al.*[27] demonstrated a significant increase of initiation thresholds with mechanical strength of tissues increasing, and the thresholds of tissues are closely related to ultimate strength, density, and water content.

It should be noted that tissue stiffness also affects the histotripsy-induced cavitation bubble behaviors. It proves that there is a significant decrease in bubble expansion and collapse time by increasing tissue phantom stiffness.[28] It is worth mentioning that the elastic moduli of different soft tissues vary greatly.[29–31] Vlaisavljevich[27] reported significantly high initiation thresholds for porcine skin, tendon, tongue, and cartilage (high mechanical strength), and relatively low thresholds for lung, fat, and kidney (low mechanical strength); while the thresholds of skeletal muscle, cardiac muscle, and liver lie between the above two thresholds. Therefore, it is necessary to consider the influence of tissue properties on nucleation, and a theory should be developed to present a more in-depth understanding of the potential nucleation probability and subsequent cavitation effects in ultrasonic diagnostic and therapeutic applications. According to previous theory proposed by Andrade *et al.*,[24,25] the soft tissue can be simplified into a fluid-filled cavity enclosed by an unbounded elastic medium, where the bulk modulus is introduced into the equation of state to account for the confining effect of elastic medium. The growth of gas nuclei in liquid micro-cavity was simplified to two "processes"[32] and it was shown that the nucleation threshold pressure is influenced by the dissolved gas in gas-containing liquids. As far as we know, most of the existing theoretical studies on classical nucleation theory are devoted to nucleation in the unbounded liquid. Here, we propose a theory to simulate the cavitation nucleation in tissue by combining nucleation theory and the boundary effects of elastic medium. The effects of tissue elasticity confinement, volume confinement and dissolved gas in liquid on the nucleation cavitation threshold are investigated. The connection between the ultrasound protocol and the energy requirements for cavitation nucleation is analyzed. Overall, it will lead to a better understanding of tissue characteristics, which is essential in advancing histotripsy, and provide a theoretical basis for guiding the optimization of parameters for specific tissue treatment.

2. Theory

2.1. Modified thresholds in cavities enclosed by elastic constraint

Following thermodynamic principles and phenomenological implementation of CNT, Andrade *et al.*[24] obtained the expression of the nucleation threshold for the emergence of Σ nuclei in a volume V_0 after a time interval τ_S as follows:

$$P_L^N = P_v - \frac{1}{\zeta}\left(\frac{16\pi\sigma^3}{3k_B T \ln\left(J_0 V_0 \tau_s/\Sigma\right)}\right)^{1/2}, \tag{1}$$

where, J_0 represents the average kinetic and spatial properties of nucleation, specifically J_0 can be expressed in the form[22] $J_0 = N_0\left(2\sigma/\pi m\right)^{1/2}$ when the effects of viscosity and inertia in the liquid are neglected, with N_0 being the number concentration of molecules with mass in the liquid phase ($N_0 \approx 3.3\times10^{22}$ cm^{-3} under room conditions); k_B is Boltzmann's constant; T is the temperature in the liquid. A brief explanation of the derivation is available in Appendix A. Equation (1) provides a method to investigate the connection between the ultrasound protocol with the energetic requirements of bubble nucleation in HIFU and the thermodynamic properties of newly nucleated bubbles.

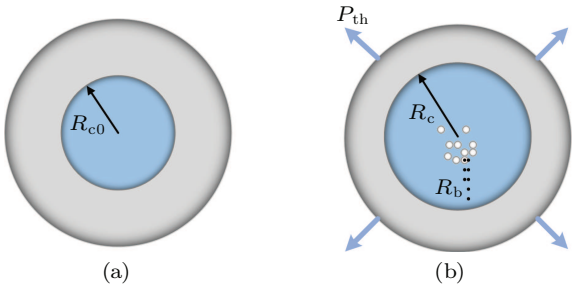


Fig. 1. Configurations of quasi-static processes of the system (schematically). A spherical liquid cavity exists in an elastic solid, where new nuclei are formed under tension P_{th}.

However, we believe that the cavitation threshold is linked to the tissue properties, and its magnitude depends on the mechanical strength and water content.[26,32] A wide range of elastic modulus values was found in both non-load bearing tissues (*e.g.*, fat, lung, and brain) and strong load bearing tissues (*e.g.*, tendons and cartilage).[29–33] Thus, the dependence of the elasticity constraint on cavitation threshold is considered. We simplify nucleation process generated in the soft tissue into that in a liquid cavity wrapped by an elastic medium. This process in the cavity is regarded as two "events", and the bulk modulus is introduced into the equation of state, representing the full confinement effect of the surrounding medium as shown in Fig. 1. Initially, at the reference state, for the undisturbed spherical cavity of radius R_{c0}, the pressure of the liquid and the pressure of the surrounding solid medium are both equal to the atmospheric pressure P_0 (Fig. 1(a)). Then, owing to the tension or negative pressure P_{th}, the liquid cell is

expanded uniformly to radius R_c ($R_c > R_{c0}$) and the new nuclei of radius R_b are formed under liquid tension P_L^N (Fig. 1(b)).

Assume that R_{b0}/R_{c0} and the liquid bulk modulus keep constant, and the pressure disturbance at the confinement wall is proportional to the change of the liquid volume, then the transient liquid pressure $P_l(V_c)$ will be expressed as[5]

$$P_l(V_c) = P_0 + \frac{K_c\left(R_c^3 - R_{c0}^3\right)}{R_{c0}^3}, \tag{2}$$

where V_{c0} and V_c are the initial and transient volumes of the liquid cavity, respectively, and K_c is the bulk modulus of liquid. The liquid pressure is P_L^N when the liquid chamber is stretched to R_c. Therefore, under elastic constraints, an external negative pressure is required to provide the threshold pressure for nucleation as follows:

$$P_{th} = P_L^N - P_0 - \frac{K_c\left(R_c^3 - R_{c0}^3\right)}{R_{c0}^3}. \tag{3}$$

When the radius of the liquid cavity is stretched from R_{c0} to R_c, Σ nuclei of radius R_b are created, and the liquid pressure P_L^N can be expressed as[32]

$$P_L^N = P_0 - \frac{K_l\left(R_c^3 - R_{c0}^3 - \Sigma R_b^3\right)}{R_{c0}^3}. \tag{4}$$

Substituting Eq. (4) into Eq. (3), the expression of R_c can be solved when the nucleation threshold pressure is obtained, and then eliminating R_c, the modified threshold pressure P_{th} can be expressed as

$$P_{th} = P_L^N - P_0 - K_c\left(\left(\frac{K_l R_{c0}^3 + P_0 R_{c0}^3 + K_l R_b^3 \Sigma}{R_{c0}^3 K_l}\right) - \frac{P_L^N}{K_l} - 1\right). \tag{5}$$

Combing Eqs. (5) and (1), and eliminating P_L^N, the modified nucleation rate under the elasticity constraint gives

$$J_s = J_0 \exp\left(-\frac{16\pi\sigma^3}{3\xi^2\left(P_v - P_{th}\right)^2 k_B T}\right). \tag{6}$$

From Eqs. (5) and (6), the cavitation threshold pressure and the steady-state nucleation rate in a liquid-filled cavity surrounded by an elastic solid medium can be estimated numerically. The liquid is assumed to be water and the inner gas of the new bubble nuclei is air. The parameters are set as follows: $P_0 = 10^5$ Pa, $R_{c0} = 100$ μm, and $T = 38$ °C. The measured bulk modulus spans a wide range spanning three orders of magnitude (21 MPa–2.37 GPa),[29–31] which also provides a reference range in computational models of biomechanics. Thus, the bulk modulus of the solid is set to $K_c = 100$ MPa unless otherwise stated. Negative pressure P is generated by pulsed ultrasound with high delivered frequency and short duration (1 μs). Despite high nucleation threshold pressure for pure liquid and soft tissues, it is possible to achieve. Nonlinear propagation of short pulsed ultrasound readily forms pulses with peak rarefactional pressure value ($P-$) in a range from 12 MPa to 25 MPa and positive shock front with peak pressures ($P+$) greater than 50 MPa,[34] and owing to the negative-pressure resulting in the superimposition of negative-pressures related to scattering and incident wave, clouds could be initiated from single cavitation bubbles formed during the initial cycles of the high-amplitude pulses of ultrasound.[35]

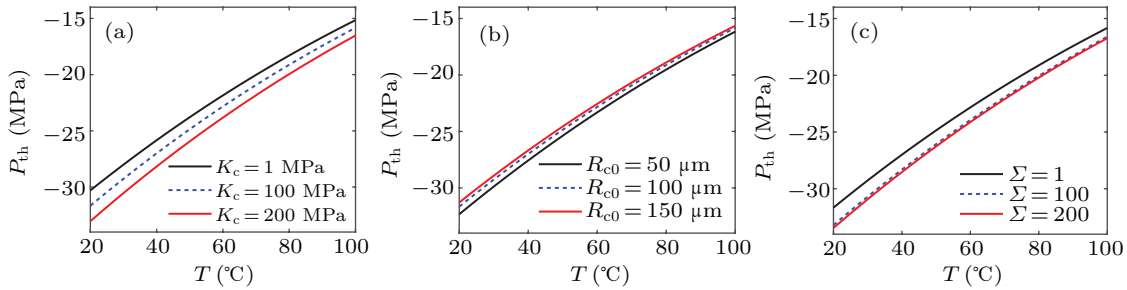


Fig. 2. Threshold pressures *versus* temperature for (a) bulk modulus of elastic medium K_c: 1, 100, and 200 MPa; (b) liquid cavity size R_{c0}: 50, 100, and 200 μm, and (c) total number of nucleation Σ: 1, 100, and 200, respectively.

The local cavitation field in soft tissues is complex, and the threshold of cavitation onset increases with the mechanical strength and density of the tissue increasing.[27] In order to verify the confining effect of the surrounding medium, the relationship between nucleation threshold pressure and temperature was simulated numerically for different bulk modulus values, cavity sizes, and nucleon numbers. In all cases shown in Fig. 2, the threshold pressure decreases with temperature increasing. The possible reasons are given as follows: firstly, the saturated vapor pressure P_v increases with temperature rising, which leads the modified nucleation rate to increase and the threshold pressure to lower. Secondly, at higher temperature, boiling nucleation is more likely to occur. At the same time, soft tissue elasticity affects the threshold of tissue cavitation nucleation.[27] By comparing the curves for $K_c = 1$ MPa, 100 MPa, and 200 MPa in Fig. 2(a), it is found that the threshold pressure increases with the enhancement of bulk modulus at a given temperature (Fig. 2(a)), which is in good agreement with the experimental measurements of Vlaisavljevich *et al.*[27] They demonstrated that the initiation threshold depends

on the type of porcine tissues and significantly higher initiation thresholds are obtained in porcine skin, tendon, tongue, and cartilage (high mechanical strength). It is should be noted that the size of the liquid cavity affects threshold pressure and the total number of nucleation. The nucleation becomes harder when the liquid cavity is shrunk (Fig. 2(b)). Supposing that the water content of the tissue is proportional to the size of the liquid, a smaller cavity may mean lower water content and more difficult nucleation.[27] Similarly, high value of nuclei nucleation rate demands a large pressure (Fig. 2(c)). It is noteworthy that once the threshold pressure required for one nucleus is available, there is a high possibility of obtaining more nuclei by a slightly increasing the negative pressure.

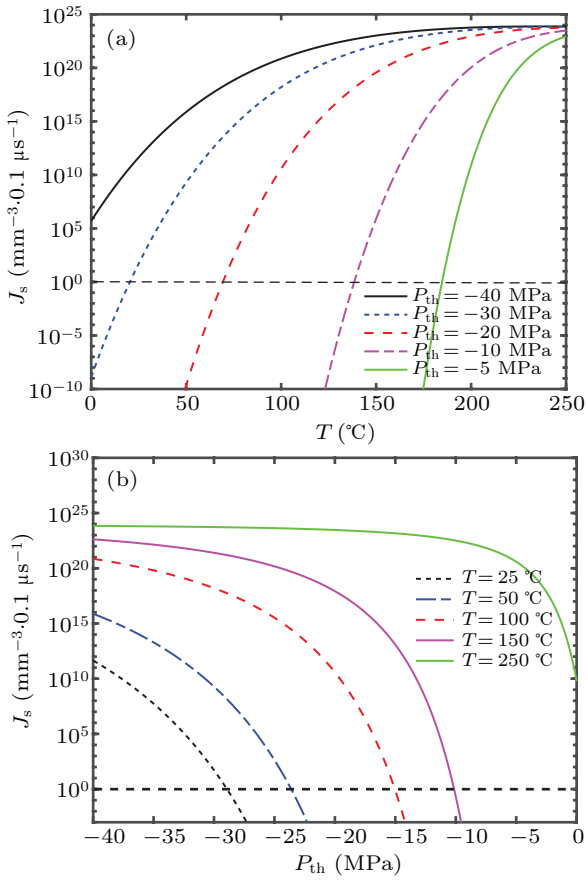


Fig. 3. Effects of (a) temperature under different pressures and (b) negative pressure at different temperatures on nucleation rate.

When the nucleation threshold is obtained, nucleation process starts, and the nucleation rate J_S is defined as the number of nuclei in a volume $V = \left(4\pi R_{c0}^3\right)/3$ after a time interval τ_S in unit of 0.1 ms per cubic millimeter. Figure 3 reveals that the temperature and negative pressure have a great influence on the steady-state nucleation rate, and a specific nucleation rate corresponds to a pair of temperature-negative pressure values. It is assumed that there is a critical nucleation rate $\Sigma/V_0\tau_S$, and if the critical value is reached the system cannot be considered as single-phase.[24] For $\Sigma = 1$, the critical nucleation threshold is the liquid pressure marked by intersect of the solid line $1/V_0\tau_S$ and the curve of Eq. (6) at a given temperature T in Fig. 3. That is to say, if nucleation rate J_S is greater than $1/V_0\tau_S$, bubbles can be formed, and *vice versa*, the onset of bubble activity is impossible.

By comparing the curves for the cases of negative pressures of −5 MPa, −10 MPa, −20 MPa, −30 MPa, and −40 MPa (Fig. 3(a)), it is shown that the higher the negative pressure, the higher the nucleation rate at a given temperature is. The nucleation rate varies smoothly with temperature and pressure, and the saturation phenomenon exists when the temperature excesses 100 °C. For a very low negative pressure with an absolute value less than 5 MPa, the nucleation temperature will exceed about 200 °C (Fig. 3(b)), which is incompatible to the cavitation onset in water due to vaporization. However, it may transiently happen in tissues under high-intensity focused ultrasound stimulation. This suggests that the tissue cavitation can be maintained by lower pressures after being excited.

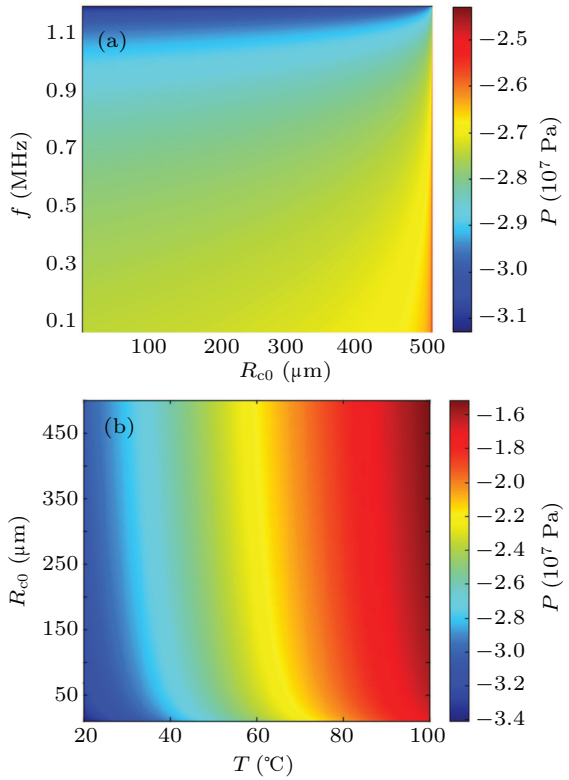


Fig. 4. Maps of nucleation thresholds, showing (a) effect of the frequency and cavity volume, and (b) effect of cavity volume and temperature.

When the ultrasound frequency increases from 345 kHz to 3 MHz, the threshold pressure increases slightly (by 2 MPa–3 MPa) in the experiments on histotripsy.[28] However, at an ultrasound frequency of 1 MHz, the nucleation threshold significantly decreases with temperature increasing, showing a nearly linear decreasing trend.[21] Therefore, temperature may have a greater influence on the nucleation process. The influences of cavity size, frequency, and temperature on the threshold pressure are shown in Fig. 4. According to the predictions

of our model, the effect of the frequency is relatively weak, probably because the nucleus process is very short and smaller than the acoustic period. Similarly, although a decrease of the pressure magnitude can be observed in the map (Fig. 4(a)), the cavity size has less influence on the process. The volume confinement does suppress the occurrence of cavitation, which is consistent with the effect of elastic confinement on Blake threshold.[5] On the contrary, temperature plays an important role in the threshold pressure (Fig. 4(b)).

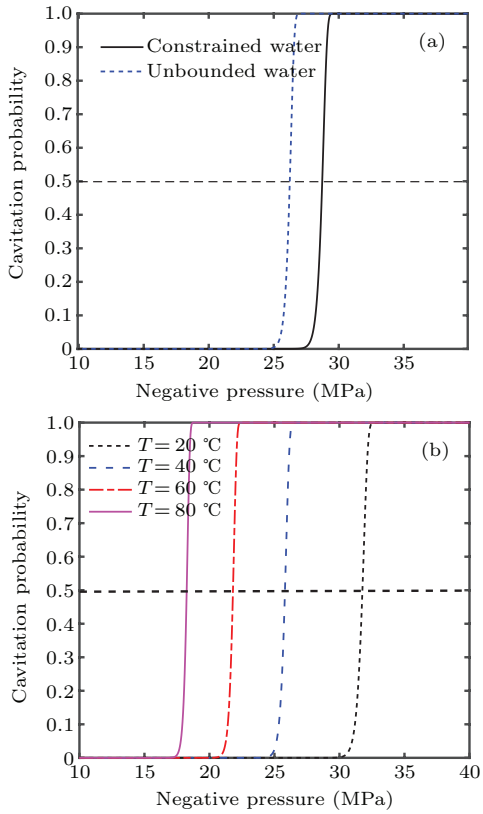


Fig. 5. Nucleation probability *versus* negative pressures: (a) effects of bulk modulus and (b) effects of temperature.

The cavitation onset at a negative acoustic pressure is a random event with a certain probability distribution. Defining the cavitation probability as the ratio of the number of cavitation events to the total number of experimental events, the cavitation probability will vary with the liquid pressure under given experimental conditions (*e.g.* the given temperature and impurity concentration). When the cavitation probability is 0.5, the liquid pressure is usually defined as the cavitation threshold pressure. Theoretically, this pressure is equal to the tensile stress required to form a critical bubble at the onset of cavitation.[20] Therefore, for the specific volume and time, the nucleation probability is defined by the classical nucleation theory as[36]

$$H = 1 - \exp(-J_S V_0 \tau_S). \tag{7}$$

The predicted thresholds are about 26.25 MPa and 28.72 MPa for unbounded liquid and the cavity enclosed by an elastic constraint ($K_c = 100$ MPa), respectively, as shown in Fig. 5(a). The difference is not so obvious when the bulk modulus is small and the confinement effect is weak. However, the cavitation probability can be improved by increasing temperature. Comparing the thresholds at 20 °C and 80 °C (Fig. 5(b)), it can be seen that the two values differ by almost half, and this trend can also be confirmed by the experimental results of Vlaisavljevich *et al.*[21]

2.2. Effects of dissolved gas

Solid particles and dissolved gases are the two main impurities in liquids.[37] At room temperature, water contains 20 ppm of nitrogen, oxygen, argon, and amounts of carbon dioxide, and many experimental results have demonstrated that the nanobubbles can survive and remain stable for hours.[38] Therefore, dissolved gases can also participate in bubble formation, so the critical cavitation threshold pressure is modified into the following expression:

$$\begin{aligned} P_{DG}^{N} &= P_{L}^{N} + P_{dg} - P_0 \\ &\quad - K_c \left[\left(\frac{K_l R_{c0}^3 + P_0 R_{c0}^3 + K_l R_b^3 \Sigma}{R_{c0}^3 K_l} \right) - \frac{P_L^N}{K_l} - 1 \right]. \end{aligned} \tag{8}$$

According to the Henry's law, the partial pressure of the dissolved gas in the bubble yields[39]

$$P_{dg} = \sum_{i}^{M} k_i C_{gi}, \tag{9}$$

where C_{gi} is the concentration of the i-th type of dissolved gas in mole fraction, k_i and M refer to the Henry's constant and the total number of dissolved gases, respectively. Henry's constant k_i is only related to gas species and ambient temperature and it is hardly influenced by the pressure. The Henry's law can only be used when the dissolved gas content is low in the working fluid. Based on this law, the gaseous cavitation effect caused by low dissolved gas content can be considered by the contribution of partial pressure.

Numerical analysis of the evolution of the threshold pressure with ultrasound frequency is shown in Fig. 6. By comparing the cases with O_2 concentration of 0, 0.002, and 0.004, it is found that the threshold increases with frequency increasing, but the slope of the curve decreases, which means that the cavitation is less likely to occur in higher frequency bands than 1 MHz. Similarly, the suppression of confining medium has a negative influence on cavitation onset, with a higher threshold pressure than that in unbounded liquid. The presence of dissolved O_2 benefits the cavitation process, and it is observed that the threshold decreases with dissolved O_2 concentration increasing, which is consistent with the measurements of Li *et al.*,[37] and they observed that the cavitation intensifies with gas concentration increasing at a given temperature and gas species.

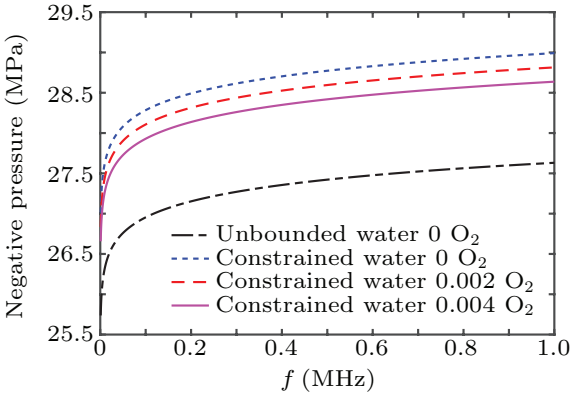


Fig. 6. Effect of frequency on nucleation threshold pressure.

If the influence of viscous force and inertial force are both small in liquid with dissolved gases, the kinetic behavior of bubble nucleation depends on the evaporation rate of vapor molecules and the diffusion rate of gas molecules on the bubble surface. If the latter factor is decisive, the net rate of bubble formation is given by[40]

$$\begin{aligned} J_{\mathrm{D}} &= N_0 \Delta P^* \left(\frac{k_{\mathrm{B}}T}{6\pi\eta r}\right)\left(\frac{\partial C}{\partial P}\right)_{P_{\mathrm{c}}}\left(\frac{k_{\mathrm{B}}T}{\sigma}\right)^{1/2} \\ &\quad \times \exp\left(-\frac{16\pi\sigma^3}{3\xi^2\left(P_{\mathrm{v}}-P+P_{\mathrm{dg}}\right)^2 k_{\mathrm{B}}T}\right) \\ &\cong N_0\left(\frac{k_{\mathrm{B}}T}{6\pi\eta r}\right)(C-C_0)\left(\frac{k_{\mathrm{B}}T}{\sigma}\right)^{1/2} \\ &\quad \times \exp\left(-\frac{16\pi\sigma^3}{3\xi^2\left(P_{\mathrm{v}}-P+P_{\mathrm{dg}}\right)^2 k_{\mathrm{B}}T}\right), \end{aligned} \tag{10}$$

where C is the concentration of dissolved gas, C_0 is the equilibrium concentration at a vapor pressure equal to the ambient pressure P_0, and $k_{\mathrm{B}}T/6\pi\eta r$ is the diffusion coefficient in liquid, r is the gas molecule radius in the liquid, and η is the coefficient of viscosity.

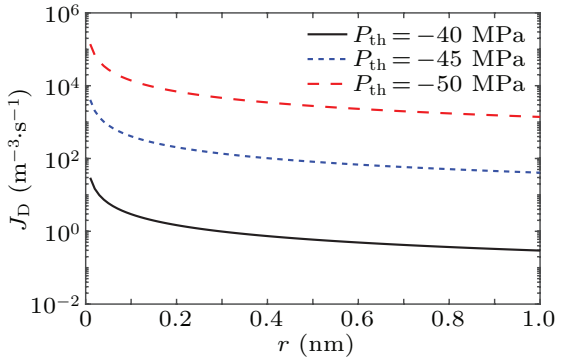


Fig. 7. Effects of molecular radius of dissolved gas on nucleation rate for negative pressures of −40 MPa, −45 MPa, and −50 MPa, respectively.

It can be clearly seen that the gas molecules radius affects the nucleation rate J_{D}, and the nucleation rate can be enhanced by the dissolved O_2 and N_2.[37] It should be mentioned that there are various types of dissolved gases in soft tissues. Here, the effect of different types of dissolved gases on the diffusion nucleation rate J_{D} is investigated using Eq. (10). There is a negative correlation between the diffusion nucleation rate J_{D} and the radius of dissolved gas as shown in Fig. 7. Comparing the diffusion nucleation rate J_{D} with the modified classical nucleation rate J_{S}, it is found that the nucleation threshold pressure increases significantly due to the gas diffusion hindering the formation of gas nuclei. The diffusion of the dissolved gas controls the growth rate of the bubble, which is associated with the hindrance of molecular vaporization, and the slowdown of the nucleation rate. Comparing Eq. (6) with Eq. (10), it is found that the exponential coefficient J_0 is influenced by the dissolved gas, the average kinetic and spatial properties of nucleation in liquid. However, it is observed that oxygenated water samples are more susceptible to cavitation than non-oxygenated ones,[37] and the theoretical threshold is larger than the experimental value. This phenomenon cannot be explained by the modified classical nucleation theory, and we predict that it may be related to the inhomogeneous nucleation. Therefore, the inhomogeneous nucleation in cavity encapsulated by elastic media should be further studied.

Here, we develop a model to explain the inhomogeneous nucleation by using the modified Blake threshold theory, which may promote a better understanding of the local cavitation nucleation phenomenon in soft tissues. It is supposed that there are many gas nuclei of R_{b} inside a spherical liquid-filled cavity as shown in Fig. 8(a). The instantaneous radii of the gas nucleus and cavity are R_{b1} and R_{c1} with initial values of R_{b} and R_{c}, respectively. The gas nucleus is driven to grow by negative pressure P_{th1}. According to the classical Blake threshold theory, the pressures at the bubble surface in an unbounded liquid satisfies

$$P_{\mathrm{l}}+\frac{2\sigma}{R_{\mathrm{b1}}} = P_{\mathrm{v}}+\left(P_0-P_{\mathrm{v}}+\frac{2\sigma}{R_{\mathrm{b}}}\right)\frac{R_{\mathrm{b}}^3}{R_{\mathrm{b1}}^3}. \tag{11}$$

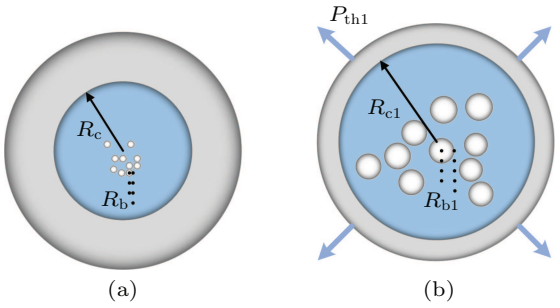


Fig. 8. Configurations of the quasi-static motion of the system: (a) elastic solid contains a spherical liquid cavity with a gas bubble nucleus and (b) growth of the cavity under tension P_{th1}.

When the gas nucleus in the liquid cavity grows to a new equilibrium state under the action of external negative pressure

P_{th1}, the equilibrium relationship of pressure on the bubble surface is obtained[32]

$$P_0 - K_{\mathrm{l}} \frac{R_{\mathrm{c1}}^3 - R_{\mathrm{c}}^3 - \Sigma\left(R_{\mathrm{b1}}^3 - R_{\mathrm{b}}^3\right)}{R_{\mathrm{c}}^3 - \Sigma R_{\mathrm{b}}^3} + \frac{2\sigma}{R_{\mathrm{b1}}} = \left(P_0 - P_{\mathrm{v}} + \frac{2\sigma}{R_{\mathrm{b}}}\right)\frac{R_{\mathrm{b}}^3}{R_{\mathrm{b1}}^3} + P_{\mathrm{v}}, \tag{12}$$

where K_{l} is the bulk modulus of the liquid. The dependence of the liquid-cavity radius on the negative pressure is given by[41]

$$\frac{R_{\mathrm{c1}}^3 - R_{\mathrm{c}}^3}{R_{\mathrm{c}}^3} = -\frac{1}{K_{\mathrm{c}}}\left(P_{\mathrm{th1}} - P_0\right) + \frac{3}{4G}\left(P_{\mathrm{l}} - P_{\mathrm{th1}}\right), \tag{13}$$

where $G = 3K_{\mathrm{c}}/4$ is the shear moduli of the elastic solid. Combining Eqs. (12) and (13), the expression of negative pressure P_{th1} can be deduced, and the detailed process is given in Appendix B. In general, P_{th1} depends on nondimensionalized radius $\overline{R}_{\mathrm{b}}$, which yields

$$P_{\mathrm{th1}} = \frac{4Q - 4\left(\overline{R}_{\mathrm{c1}}^3/\overline{R}_{\mathrm{c}}^3 - 1\right) + 3H\overline{P}_{\mathrm{l}}}{3H + 4Q} P_0, \tag{14}$$

where

$$\overline{R}_{\mathrm{b}} = \frac{P_0 R_{\mathrm{b}}}{2\sigma}, \quad \overline{R}_{\mathrm{c}} = \frac{P_0 R_{\mathrm{c}}}{2\sigma}, \quad \overline{R}_{\mathrm{b1}} = \frac{P_0 R_{\mathrm{b1}}}{2\sigma},$$
$$\overline{R}_{\mathrm{c1}} = \frac{P_0 R_{\mathrm{c1}}}{2\sigma}, \quad \overline{P}_{\mathrm{v}} = \frac{P_{\mathrm{v}}}{P_0}, \quad A = 1 - \overline{P}_{\mathrm{v}} + \frac{1}{\overline{R}_{\mathrm{b}}},$$
$$B = \frac{K_{\mathrm{l}}}{P_0}, \quad Q = \frac{P_0}{K_{\mathrm{c}}}, \quad H = \frac{P_0}{G},$$
$$\overline{P}_{\mathrm{l}} = A\left(\frac{\overline{R}_{\mathrm{b}}}{\overline{R}_{\mathrm{b1}}}\right)^3 - \frac{1}{\overline{R}_{\mathrm{b1}}} - \overline{P}_{\mathrm{v}}.$$

The dependence of the negative pressure on the bubble radius is given by Fig. 9, where A and B on the curve of $R_{\mathrm{b}} = 20$ nm correspond to stable state and the critical state of the growing bubble nucleus, respectively. In terms of negative pressure, the nuclei grow as the absolute value of the pressure increases. When the pressure increases to a critical value at B, the nuclei abruptly grow to the finite size indicated by C. If the pressure decreases, the finite-sized bubbles are shrinking along the curve from C to D, and then collapse to size A. Therefore, the cavitation threshold is denoted by the pressure at B. By comparing the curves for $R_{\mathrm{b}} = 0.8$ nm, 5 nm, 10 nm, and 20 nm, it is found that the sizes of the gas nuclei have a significant effect on the cavitation threshold, and the threshold increases with the radius of the gas nucleus decreasing. The cavitation threshold of 0.8 nm nucleus is about −21 MPa, which is consistent with the experimental values (−16 MPa ∼ −27 MPa).[27] Moreover, when the nucleus is 20 nm, the threshold deceases to less than 1 MPa. The experimental thresholds may be influenced by the impurities in the water. Dissolved gases are the most common impurities in water, especially oxygen and nitrogen with a molecular radius of about 0.2 nm. The dissolved gas molecules attract each other and aggregate into bubble nuclei. Dissolved gases are present in the liquid of biological tissues; therefore, the modified Black's threshold model, Eq. (14), can be used to explain the phenomenon of the cavitation in biological tissues.

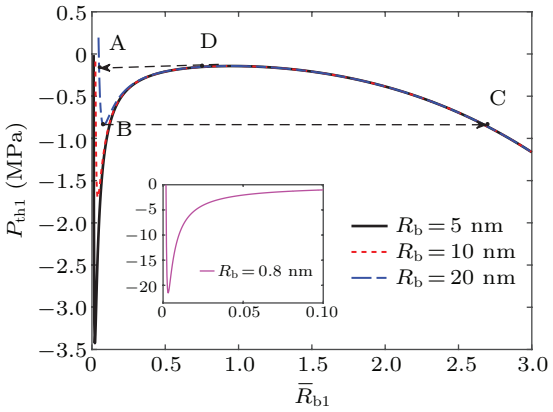


Fig. 9. Variations of negative pressure with $\overline{R}_{\mathrm{b1}}$ of nuclei for different values of R_{b}.

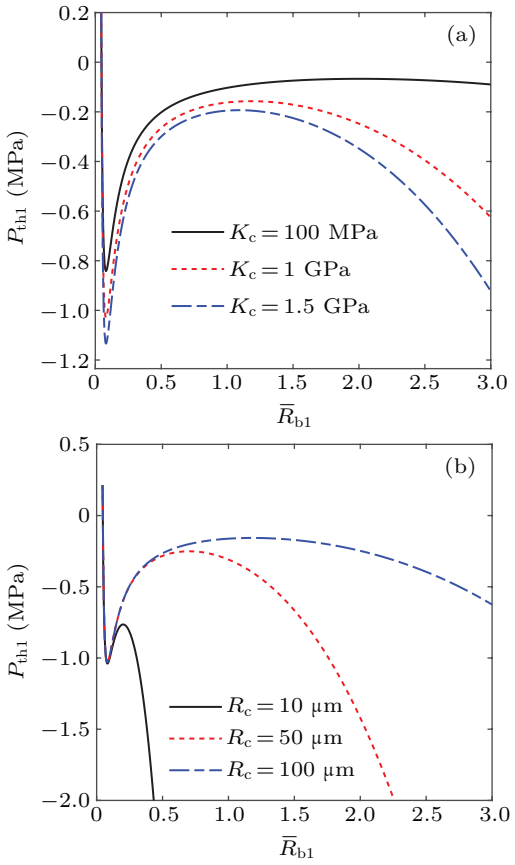


Fig. 10. Curves of negative pressure *versus* bubble radius, with (a) bulk modulus of elastic medium being 1 MPa, 1 GPa, and 1.5 GPa, respectively, and (b) with initial radius of the cavity being 10 μm, 50 μm, and 100 μm, respectively.

To better understand the influence of the surrounding medium, we simulate the threshold pressures by setting the bulk modulus to 100 MPa, 1 GPa, and 1.5 GPa, respectively,

and the nucleus radius to 20 nm, as shown in Fig. 10(a). It is seen that the threshold pressure increases with the bulk modulus increasing, and the same conclusion was obtained from Fig. 2(a). The stable radii of the nuclei for the three cases are almost equal, while the maximum radius of the expanding nucleus decreases with bulk modulus increasing, which implies that the physical properties of the medium do affect the cavitation behaviors, especially on the growth and kinetic behavior of the bubbles.[6] Similarly, the liquid cavity size affects the response of a single gas nucleus.[5] The simulations in Fig. 10(b) reveal that the smaller the liquid cavity, the smaller the equilibrium radius of the nucleus is. In the presence of negative pressure, Vincent *et al.*[42] have found that the nucleus number in a gel-encapsulated liquid micro-cavity decreases with cavity size increasing, which is consistent with the theoretical prediction of our modified model in Eq. (14), indicating that liquid cavity confinement inhibits the nucleation and cavitation of gas nuclei as indicated in Fig. 8.

3. Conclusions

Cavitation behaviors in biological tissues have proved to be different from that in unbounded liquid because tissue properties affect the cavitation nucleation process. In addition, impurities in the fluid may play a key role in the experimental cavitation threshold, which is much less than the theoretical value. In this work, we developed models to describe the nucleation process in tissue by considering the tissue elasticity. Classical nucleation theory is modified to investigate the bubble nucleation in liquid-filled cavity wrapped by elastic medium, and a bulk modulus-dependent expression of the nucleation pressure threshold is derived. The importance of elastic confinement of the solid in nucleation pressure thresholds is discussed, and it is found that there is a negative correlation between the cavitation nucleation efficiency and the tissue elasticity. Based on the modified Blake threshold model, the growth process of gas nuclei induced by negative pressure is investigated, revealing that the threshold pressure and nucleation efficiency can be influenced by many factors, such as the size of the liquid cavity, temperature, the bulk modulus, acoustic frequency, and the number of nucleation. A lower nucleation threshold pressure may be obtained for a higher temperature, lower bulk modulus, larger size of the liquid cavity, and lower acoustic frequency. The nucleus process can be featured by the number of nuclei, which has a greater effect when the number is small. As a result, the nucleation rate is dominated by the temperature at $T > 100$ °C, while the nucleation is mainly controlled by the negative pressure at $T < 100$ °C. The predicted nucleation threshold pressure accords well with the experimental result. The dissolved gas has an influence on cavitation nucleation, and the inhomogeneous nucleation is simulated. The numerical analysis shows that the nucleation threshold pressure of gas nuclei with an initial radius of 0.8 nm at room temperature is −21 MPa, and the threshold pressure decreases with the radius of gas nuclei increasing.

Appendix A: Theory of nucleation

Provided in this appendix is a brief explanation of classical nucleation theory. The critical work of nucleation W^* is[42]

$$W^* = \frac{16\pi}{3}\frac{\sigma^3}{(P' - P_\mathrm{l})^2}, \tag{A1}$$

where σ is the surface tension of liquid, P_l is the pressure in the liquid, P' is the pressure inside a newly formed vapour nucleus.

At the critical size, the steady-state nucleation rate is usually expressed as[18]

$$J_\mathrm{S} = J_0 \exp\left(-W^*/k_\mathrm{B}T\right), \tag{A2}$$

the factor J_0 before the exponential expression represents the average kinetic and spatial properties of nucleation. By neglecting the effects of viscosity and inertia in the liquid, J_0 can be expressed as[19] $J_0 = N_0\left(2\sigma/\pi m\right)^{1/2}$, where N_0 is the number concentration of molecules with mass m in the liquid phase, specifically, $N_0 \approx 3.3 \times 10^{22}$ cm^{-3} at room conditions. In Eq. (A2), k_B is Boltzmann's constant, and T is the temperature in the liquid.

Because the P_l and T are transient values in the acoustic field, considering the formation of the first Σ nuclei, the phenomenological nucleation rate J_S for the appearance of nuclei in a volume J_S after time τ_S (in units of s) is given by[20]

$$J_\mathrm{S} = \frac{\Sigma}{V_0\tau_\mathrm{S}}. \tag{A3}$$

Let the thermodynamic expression (Eq. (A2)) equal the phenomenological expression (Eq. (A3)) for the nucleation rate, replace the critical work of nucleation given by Eq. (A1) and solve the resulting expression, then the correction nucleation pressure threshold will be obtained as follows:[20]

$$P_\mathrm{L}^\mathrm{N} = P_\mathrm{v} - \frac{1}{\zeta}\left(\frac{16\pi\sigma^3}{3k_\mathrm{B}T\ln\left(\frac{J_0V_0\tau_\mathrm{s}}{\Sigma}\right)}\right)^{1/2}, \tag{A4}$$

where

$$\zeta = 1 - \left(\frac{\rho_\mathrm{v}}{\rho_\mathrm{l}}\right) + \frac{1}{2}\left(\frac{\rho_\mathrm{v}}{\rho_\mathrm{l}}\right)^2,$$

and ρ_v and ρ_l denote the saturated densities of vapour and liquid. In the liquid, the vapor pressure of the liquid, P_v, vapour density ρ_l, and vapour phase are evaluated at the initial bulk

temperature of the system, according to the International Association for the Properties of Water and Steam (IAPWS).[43] It is common to approximate σ with a temperature-dependent planar surface tension $\sigma_\infty(T)$ in CNT.[43] For matching experiments, a temperature-dependent scaling factor $c_{\rm E}(T)$ for the surface tension is calculated from $\sigma_{\rm E}(T) = c_{\rm E}(T)\sigma_\infty(T)$. For temperature values $0\ ^\circ\text{C} < T < 90\ ^\circ\text{C}$, $c_{\rm E}(T)$ is extrapolated based on $c_{\rm E}(T) = 0.4869 - 6.1425 \times 10^{-4}(T + 273.15)$. For temperature values above 110 °C, taking a conservative approach and assuming $c_{\rm E}(T)$ to be constant, then $c_{\rm E}(T > 110\ ^\circ\text{C}) = c_{\rm E}(110\ ^\circ\text{C})$ will hold true.[20]

Appendix B: Modified Blake model

According to the classical Blake threshold theory, the relationship of the pressures on the bubble surface in an unbounded liquid satisfies

$$P_{\rm l}+\frac{2\sigma}{R_{\rm b1}} = P_{\rm v} + \left(P_0 - P_{\rm v} + \frac{2\sigma}{R_{\rm b}}\right)\frac{R_{\rm b}^3}{R_{\rm b1}^3}. \tag{B1}$$

As shown in Fig. 8, Σ gas nuclei grow under the negative pressure $P_{\rm th1}$, the liquid pressure in the liquid cavity can be expressed as[28]

$$P_{\rm l} = P_0 - K_{\rm l}\frac{R_{\rm c1}^3 - R_{\rm c}^3 - \Sigma\left(R_{\rm b1}^3 - R_{\rm b}^3\right)}{R_{\rm c}^3 - \Sigma R_{\rm b}^3}. \tag{B2}$$

In static equilibrium, the bubble pressure is balanced with this altered ambient liquid pressure $P_{\rm l}$, Laplace pressure due to surface tension, gas pressure inside the bubble and saturated vapor pressure. This balance can be presented in the following form:[28]

$$\begin{aligned} &P_0 - K_{\rm l}\frac{R_{\rm c1}^3 - R_{\rm c}^3 - \Sigma\left(R_{\rm b1}^3 - R_{\rm b}^3\right)}{R_{\rm c}^3 - \Sigma R_{\rm b}^3} + \frac{2\sigma}{R_{\rm b1}} \\ &= \left(P_0 - P_{\rm v} + \frac{2\sigma}{R_{\rm b}}\right)\frac{R_{\rm b}^3}{R_{\rm b1}^3} + P_{\rm v}, \end{aligned} \tag{B3}$$

where $K_{\rm l}$ is the bulk modulus of the liquid. The relationship between the liquid-cavity radius and the negative pressure is given by[39]

$$\frac{R_{\rm c1}^3 - R_{\rm c}^3}{R_{\rm c}^3} = -\frac{1}{K_{\rm c}}\left(P_{\rm th1} - P_0\right) + \frac{3}{4G}\left(P_{\rm l} - P_{\rm th1}\right). \tag{B4}$$

To simplify the analysis, the above Eqs. (B3) and (B4) are are non-dimensionalized as follows:

$$\frac{\overline{R}_{\rm c1}^3 - \overline{R}_{\rm c}^3}{\overline{R}_{\rm c}^3} = -Q\left(\overline{P}_{\rm th1} - 1\right) + \frac{3H}{4}\left(\overline{P}_{\rm l} - \overline{P}_{\rm th1}\right), \tag{B5}$$

$$1 - B\frac{\overline{R}_{\rm c1}^3 - \overline{R}_{\rm c}^3 - \Sigma\left(\overline{R}_{\rm b1}^3 - \overline{R}_{\rm b}^3\right)}{\overline{R}_{\rm c}^3 - \Sigma\overline{R}_{\rm b}^3} + \frac{1}{\overline{R}_{\rm b1}} = A\left(\frac{\overline{R}_{\rm b}}{\overline{R}_{\rm b1}}\right)^3 - \overline{P}_{\rm v}, \tag{B6}$$

where

$$\begin{aligned} &\overline{R}_{\rm b} = \frac{P_0 R_{\rm b}}{2\sigma},\quad \overline{R}_{\rm c} = \frac{P_0 R_{\rm c}}{2\sigma},\quad \overline{R}_{\rm b1} = \frac{P_0 R_{\rm b1}}{2\sigma}, \\ &\overline{R}_{\rm c1} = \frac{P_0 R_{\rm c1}}{2\sigma},\quad \overline{P}_{\rm v} = \frac{P_{\rm v}}{P_0},\quad A = 1 - \overline{P}_{\rm v} + \frac{1}{\overline{R}_{\rm b}}, \\ &B = \frac{K_{\rm l}}{P_0},\quad Q = \frac{P_0}{K_{\rm c}},\quad H = \frac{P_0}{G},\quad \overline{P}_{\rm th1} = \frac{P_{\rm th1}}{P_0}. \end{aligned}$$

To simplify the analysis, equation (B5) is rewritten in the form of negative pressure $\overline{P}_{\rm th1}$ by using Eq. (B6):

$$P_{\rm th1} = \frac{-4\left(\frac{\overline{R}_{\rm c1}^3 - \overline{R}_{\rm c}^3}{\overline{R}_{\rm c}^3}\right) + 3H\overline{P}_{\rm l} + 4Q}{3H + 4Q}. \tag{B7}$$

Acknowledgement

Project supported by the National Natural Science Foundation of China (Grant Nos. 11974232 and 11727813).

References

[1] Wu X Y and Liang J F 2021 *Acta Phys. Sin.* **70** 184301 (in Chinese)
[2] Wang C H, Mo R Y, Hu J and Zhang M D 2017 *Sci. Sin.-Phys. Mech. Astron.* **47** 024301 (in Chinese)
[3] Mo R Y, Wang C H, Hu J and Chen S 2019 *Acta Phys. Sin.* **68** 144302 (in Chinese)
[4] Guo C, Zhu X J, Wang J Q and Ye L Z 2016 *Acta Phys. Sin.* **65** 044304 (in Chinese)
[5] Zhang X M, Wang C H, Guo J Z, Mo R Y, Hu J and Chen S 2021 *Acta Phys. Sin.* **70** 214305 (in Chinese)
[6] Zhang X M, Li F, Wang C H, Guo J Z, Mo R Y, Hu J, Chen S, He J X and Liu H H 2022 *Ultrason Sonochem* **84** 105957
[7] Kennedy J E 2005 *Nat. Rev. Cancer* **5** 321
[8] Matsumoto Y, Allen J S, Yoshizawa S, Ikeda T and aneko Y 2005 *Experimental Thermal and Fluid Science* **29** 255
[9] Maxwell A 2012 *Noninvasive Thrombolysis Using Histotripsy Pulsed Ultrasound Cavitation Therapy*, Ph. D. dissertation
[10] Lentacker I, De Cock I, Deckers R, De Smedt S C and Moonen C T 2014 *Adv. Drug. Deliv. Rev.* **72** 49
[11] Coussios C C and Roy R A 2008 *Annual Review of Fluid Mechanics* **40** 395
[12] Brennen C E 2015 *Interface Focus* **5** 20150022
[13] Poon C, McMahon D and Hynynen K 2017 *Neuropharmacology* **120** 20
[14] Miller D L, Smith N B, Bailey M R, Czarnota G J, Hynynen K and Makin I R S 2012 *Journal of Ultrasound in Medicine* **31** 623
[15] Fisher J C 1948 *J. Appl. Phys.* **19** 1062
[16] Kwak H Y and Panton R L 1985 *J. Phys. D: Appl. Phys.* **18** 647
[17] Bader K B and Vlaisavljevich E, Maxwell A D 2019 *Ultrasound Med Biol* **45** 1056
[18] Herbert E, Balibar S and Caupin F 2006 *Phys. Rev E.* **74** 041603
[19] Davitt K, Arvengas A and Caupin F 2010 *Europhys. Lett.* **90** 16002
[20] Maxwell A D, Cain C A, Hall T L, Fowlkes J B and Xu Z 2013 *Ultrasound Med. Biol.* **39** 449
[21] Vlaisavljevich E, Xu Z, Maxwell A, Mancia L, Zhang X, Lin K W, Duryea A, Sukovich J, Hall T, Johnsen E and Cain C 2016 *IEEE Trans. Ultrason. Ferroelectr. Freq. Control* **63** 1064
[22] Blander M and Katz J L 1975 *AIChE Journal* **21** 833
[23] Hanna V 2006 *Classical Nucleation Theory in Multicomponent Systems* (Berlin: Springer-Verlag) pp. 7–26
[24] de Andrade M O, Haqshenas S R, Pahk K J and Saffari N 2019 *Ultrason Sonochem* **55** 262
[25] de Andrade M O, Haqshenas R, Pahk K J and Saffari N 2022 *Ultrason Sonochem.* **88** 106091
[26] Vlaisavljevich E, Kim Y, Owens G, Roberts W, Cain C and Xu Z 2014 *Phys. Med. Biol.* **59** 253
[27] Vlaisavljevich E, Cain C A and Xu Z 2011 *IEEE International Ultrasonics Symposium*, IUS, October 18–21 2011, Orlando, USA, 1490

[28] Vlaisavljevich E, Lin K W, Warnez M T, Singh R, Mancia L, Putnam A J, Johnsen E, Cain C and Xu Z 2015 *Phys. Med. Biol.* **60** 2271
[29] Saraf H, Ramesh K T, Lennon A M, Merkle A C and Roberts J C 2007 *Experimental Mechanics* **47** 439
[30] Saraf H, Ramesh K T, Lennon A M, Merkle A C and Roberts J C 2007 *J. Biomech.* **40** 1960
[31] Ganpule S, Daphalapurkar N P, Cetingul M P and Ramesh K T 2018 *Shock Waves* **28** 127
[32] Leonov K and Akhatov I 2020 *International Journal of Multiphase Flow* **130** 103369
[33] Vincent O and Marmottant P 2017 *J. Fluid Mech.* **827** 194
[34] Khokhlova V A, Fowlkes J B, Roberts W W, Schade G R, Xu Z, Khokhlova T D, Hall T L, Maxwell A D, Wang Y N and Cain C A 2015 *Int. J. Hyperthermia* **31** 145
[35] Maxwell A D, Wang T Y, Cain C A, Fowlkes J B, Sapozhnikov O A, Bailey M R and Xu Z 2011 *J. Acoust. Soc. Am.* **130** 1888
[36] Qin D, Zou Q, Lei S, Wang W and Li Z 2021 *Ultrason Sonochem.* **75** 105608
[37] Li B, Gu Y and Chen M 2017 *Experiments in Fluids* **58** 164
[38] Li M Z, Xing Y W, Li J Z and Jun H U 2021 *Scientia Sinica Physica, Mechanica & Astronomica* **51** 092006
[39] Li D, Liu S, Wei Y, Ren T and Tang Y 2018 *Int. Commun. Heat Mass Transfer* **97** 17
[40] Blander M and Katz J L 1975 *AIChE Journal* **21** 833
[41] Leonov K and Akhatov I 2021 *Phys. Rev. E* **104** 015105
[42] Vincent O, Marmottant P, Gonzalez-Avila S R, Ando K and Ohl C D 2014 *Soft Matter* **10** 1455
[43] Caupin F and Herbert E 2006 *Comptes Rendus Physique* **7** 1000
[44] Wagner W and Pruß A 2002 *Journal of Physical and Chemical Reference Data* **31** 387